Two-Level Power Combining Using a Lens Amplifier

Jon S. H. Schoenberg, *Member, IEEE*, Scott C. Bundy, *Student Member, IEEE*, and Zoya B. Popović

Abstract— **A two-level quasi-optical power combiner is presented. The combiner consists of a grid oscillator which feeds a transmission amplifier at its focal point. The focal-point feed improves power coupling efficiency over that of a plane-wave feed. A linear 7-element lens amplifier array demonstrates 29 dB of isolation and a 30° continuous scan angle with less than 1 dB power variation at 9.7 GHz. A 24-element two-dimensional lens amplifier array fed by a grid oscillator demonstrates 5.7 dB gain and a 30° scan angle with less than 2dB power variation at 10.25 GHz. When horn-fed, the 24-element lens has an isolation of 17–21 dB over a 3% bandwidth. The grid oscillator, as well as receive and transmit sections of the lens amplifiers, are each fabricated on single substrates, making monolithic millimeter-wave integration of each component possible.**

I. Introduction

FREE-SPACE power combining is a technique for producing a significant amount of power at high frequencies from a large number of solid-state devices. Both self-locked [1] and injection-locked [2] oscillator power combiners have been demonstrated. A transmission amplifier has been demonstrated in which the input-to-output isolation is provided by polarization separation [3], and a polarization-flexible transmission-wave amplifier array was reported in [4]. Both amplifiers require a feed location in the far-field of the array, and thus the aperture captures only a small fraction of the total incident wave power due to diffraction losses. A more efficient input is a focal-point feed, in which the transmission amplifier works as a planar Rotman lens with active device amplification. Passive lenses using arrays of input and output antenna elements fabricated on separate substrates have been reported [5], [6]. We present two active planar lens amplifiers with a focal-point feed which improves input power coupling. The lenses are each fabricated on a single substrate containing receive and transmit arrays of microstrip patch antennas, and pseudomorphic high electron mobility transistor (PHEMT) amplifiers. We first demonstrate a linear 7-element lens amplifier array to test the concept of active lens arrays [7]. We then design a grid oscillator feeding a two-dimensional lens amplifier. This subsystem demonstrates a two-level power combiner. At the first level, a grid of transistor oscillators power combine coherently in free space, and at the second level, the oscillator power is amplified and focused by the lens amplifier.

Manuscript received April 5, 1994; revised June 17, 1994. This work was supported in part by the Army Research Office under contract number DAAL03-92-G-0265 and in part by the National Science Foundation under a Presidential Faculty Fellow Award.

The authors are with the University of Colorado, Department of Electrical and Computer Engineering, Boulder, CO 80309 USA.

IEEE Log Number 9405435.

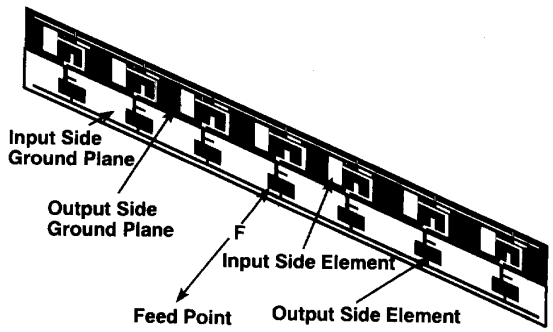

Fig. 1. The linear 7–element lens amplifier array with a focal-point feed. A horn illuminates the input side of the lens from the focal length $F = 2D$, where D is the lens length.

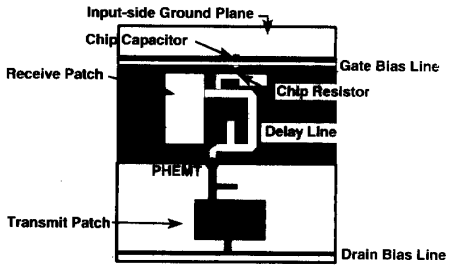

Fig. 2. Topology of a single element antenna pair used in the lens array.

II. Linear 7-Element Lens Amplifier Array

A linear 7-element lens amplifier array was designed for 10 GHz using a 0.787-mm thick Arlon substrate with a relative permittivity of 2.2. The lens amplifier, as shown in Fig. 1, has an array of receive and transmit patch antennas on opposite sides of the substrate. Each common-source PHEMT amplifier is coupled and matched to its input and output patch elements with microstrip lines. A substrate via connects each amplifier's output to its transmit-side patch. Alternating ground planes effectively isolate input and output sides of the amplifier structure, allowing input and output wave polarizations to be arbitrarily selected [4]. In the amplifier presented, orthogonal polarizations are chosen to minimize diffraction-path measurement errors.

The lens amplifier element topology is shown in Fig. 2. Receive and transmit elements are microstrip patch antennas with non-radiating-edge feeds. This is preferable to a radiating-edge feed because the element is more compact and the input impedance may be arbitrarily set. An input impedance of 100 Ω was chosen. The patches were designed using multi-

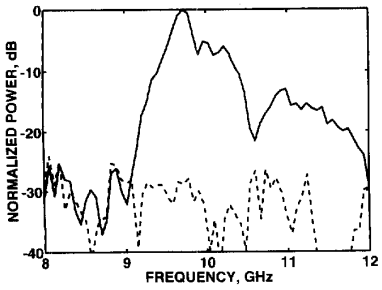

Fig. 3. Measured frequency response of the linear 7-element lens amplifier in the biased-on (solid line) and biased-off (dashed line) conditions. The on/off isolation is 29 dB.

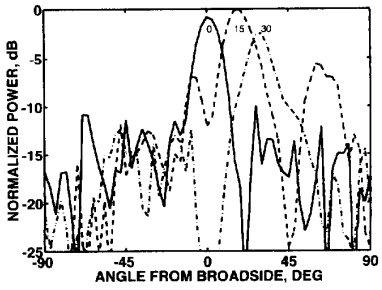

Fig. 4. Measured beamsteering performance of the linear 7-element lens amplifier array. The lens is fed at $F = 26$ cm at 0°, 15°, and 30°. The main lobe beamwidth broadens, the side lobe level increases, and the peak power varies by 2.5 dB as the beam is scanned from 0° to 30°.

port network modeling software [8]. Avantek ATF-35576 PHEMT's were selected for their high gain and low bias power requirements. The PHEMT's are impedance matched for gain to 100-Ω microstrip delay lines using single-stub matching sections. The gate bias network is similar to that described in [9], and provides unconditional stability for the PHEMT's. The gate bias network consists of a 90° section of 150-Ω microstrip line, terminated by a 70-Ω 90° open stub in parallel with a 100-Ω chip resistor connected to the gate bias line. The 1-pF chip capacitor couples the resistive stability network to the feed-side ground plane. Drain bias is provided through the RF null of the transmit patch. Each microstrip delay line has the same number of discontinuities (mitred bends) for reproducible control of phase delay.

The lens' focal length-to-diameter ratio was chosen to be $F/D = 2.0$ in order to match the radiation pattern of the feed horn. The inter-element spacing is $0.75\lambda_0$ on the transmit side, and the focal length is 27 cm. Since the input and output arrays are planar, the only Rotman lens design parameters are the relative location between receive and transmit elements, and the electrical line length connecting them. Following [5], the relative location of the input-side elements to the output-side elements is

$$\rho = r\left[\frac{F^2 - r^2\sin^2\theta_0}{F^2 - r^2}\right]^{1/2} \tag{1}$$

where ρ and r are the distances from the lens center to the input and output elements, respectively, F is the focal length, and θ_0 is the focal point angle off of broadside. The expression for the electrical line length, W, is

$$W = F + W_0 - 1/2[F^2 + \rho^2 - 2\rho F\sin\theta_0]^{1/2} - 1/2[F^2 + \rho^2 + 2\rho F\sin\theta_0]^{1/2} \tag{2}$$

where W_0 is an arbitrary constant electrical length. The center element of the feed and aperture arrays of the lens is considered to be on the lens axis. The transmit-side inter-element spacing is uniform, and thus the receive element location is a function of its corresponding transmit element position away from the lens center. The electrical line length required for the delay line is also a function of distance away from the lens center, with the longest delay line required for the center element. Electrical line length was converted into microstrip phase delay in the lens design, and as seen in Fig. 1, the delay line length decreases away from the lens axis.

At the design focal point distance of 27 cm, the lens was horn-fed and first tested with the center 5 elements biased, and then with all 7 elements biased. The resulting output power is 3.1 dB higher for 7 elements than for 5 elements biased. This is 0.2 dB above the theoretical increase of 2.9 dB ($20\log_{10}(7/5)$) expected from a uniformly driven array factor, and indicates that the output of the planar lens has a uniform phase and that its effective area increases linearly with the number of elements. Fig. 3 shows the array's maximum output power at 9.70 GHz, which is 3% below the design frequency due to the lower than expected resonant frequency of the microstrip patch antennas. The array's isolation, defined as the biased-on to biased-off transmission power ratio, is 29 dB at center frequency. The effect of the feed distance on the radiation pattern of the lens was also measured, with the feed horn located at broadside and the feed distance ranging from 22 cm to 30 cm. The 22-cm feed location produces about 5 dB more power than at 30 cm (due to different incident power) and the beamwidth is 18° compared to 14°, respectively. The theoretical beamwidth for a 7-element uniformly illuminated array is 14.6°. The wider beamwidth for the 22-cm feed location indicates that more feed power is illuminating the center element. The side lobe level is about −12 dB, compared to −12.6 dB for a 7-element uniformly driven array. The cross-polarization ratio is 19.4 dB for the 22-cm feed location, and 14.0 dB for the 27-cm feed location.

The lens preserves the incident phase of the input wave, so it may be fed with a progressive phase angle for beamsteering. Fig. 4 shows measured radiation patterns for a feed point distance of 26 cm and feed angles of 0°, 15°, and 30°. Side-lobe levels increase with increased scan angle, as expected, due to non-uniform illumination of the input elements. The main lobe power decreased by 2.5 dB from the 0° feed angle to the 30°. The difference in power is due to feeding the lens at a constant focal distance of 26 cm, independent of feed angle. Since the lens is no longer fed at its focal point at angles other than 0°, lens defocusing due to path length errors in its feed reduces the output power of the lens. Consider the diagram in Fig. 5(a), in which the lens has perfect focal points

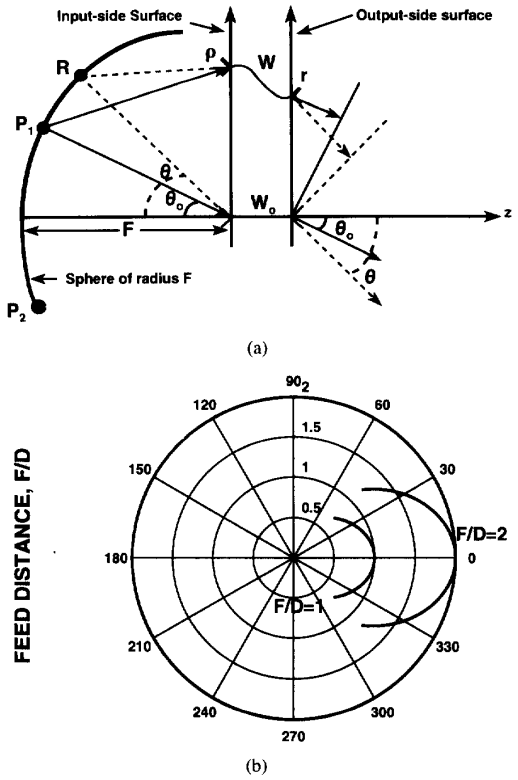

Fig. 5. The lens geometry for determining the path length error is shown in (a). The calculated focal arcs for $F/D = 1$ and $F/D = 2$ are shown in (b). The smaller F/D requires more path length error correction.

at positions P_1 and P_2 along a sphere of radius F and focal angle θ_0. The path length equality condition from focal point P_1 requires

$$\sqrt{F^2 + \rho^2 - 2F\rho\sin\theta_0} + r\sin\theta_0 + W = F + W_0. \quad (3)$$

The path length equality condition from an arbitrary feed point R along the sphere subtending an angle θ from the optical axis is of the same form as (3). The path length error ΔL at point R is the difference in the path length equations for points R and P_1. Subtracting the two expressions for the path length error condition and assuming that the focal point is on-axis ($\theta_0 = 0$), we obtain:

$$\Delta L = \sqrt{F^2 + \rho^2 - 2F\rho\sin\theta} + r\sin\theta - \sqrt{F^2 + \rho^2}. \quad (4)$$

A feed location G can be chosen at a distance different than F to minimize the peak error for any scan angle θ. Since the maximum path length error occurs at maximum r (at the aperture edge), set r to half the aperture diameter, or in terms of focal length, $r_{\max} = 0.25$ F for this lens. Using $\alpha = \sin^{-1}(r_{\max}/F)$, and following the development in [5], the path length error becomes

$$\Delta L = G - F = \sqrt{G^2 - 2FG\tan\alpha\sin\theta + F^2\tan^2(\alpha)} + F\sin\alpha\sin\theta - F\sec\alpha. \quad (5)$$

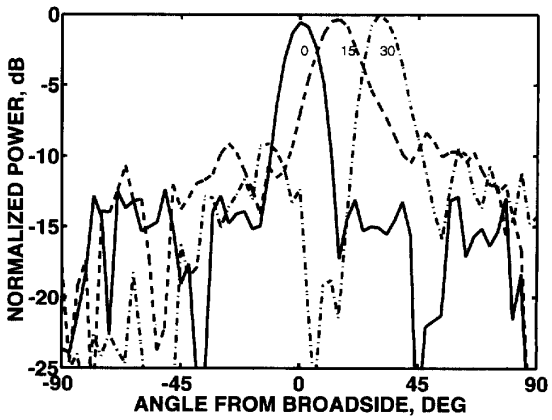

Fig. 6. Measured beamforming performance when the lens is fed along the focal arc. The beamwidth of the main lobe remains narrow, side lobe levels are reduced, and peak power variation is less than 1 db over the 30° scan range.

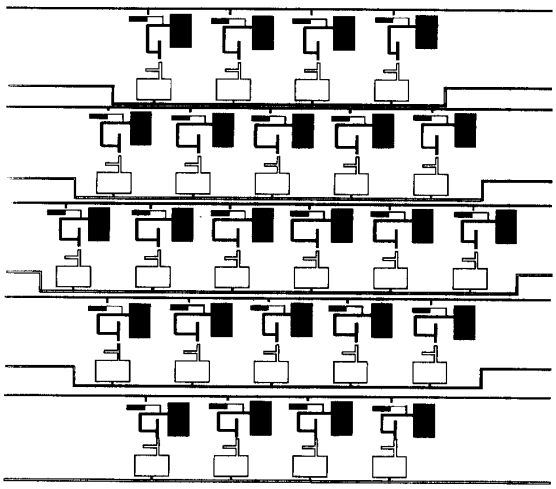

Fig. 7. A 24-element two-dimensional lens amplifier array. The lens diameter is around $4\lambda_0$, the focal length is 25cm, and the $F/D = 2$. The dark patches are on the input side, and the outlined circuitry is on the output side of the substrate.

Rearranging (5) and squaring both sides results in a solution for $G(\theta)$:

$$G(\theta) = F\left[1 + \frac{\sin^2\alpha\sin^2\theta}{2(1-\sec\alpha)(1+\sin\alpha\sin\theta)}\right]. \quad (6)$$

Fig. 5(b) shows the calculated focal arc for $F/D = 1$ and $F/D = 2$. The smaller F/D requires more path length error correction. Fig. 6 shows the improved beamforming performance as a result of feeding the lens along the focal arc. The beamwidth of the main lobe remains narrow, the side lobe levels are reduced compared to Fig. 4, and the peak power variation is less than 1 dB over the 30° scan range.

III. Two-Dimensional Lens Amplifier

Since a linear antenna array has an array factor in only one dimension, the linear transmission amplifier lens does not have absolute power gain. To eliminate diffraction loss, a 24-element two-dimensional array, shown in Fig. 7, was

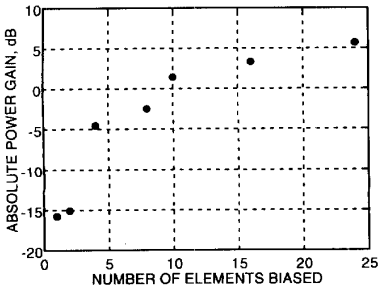

Fig. 8. Absolute power gain (or loss) of the lens amplifier array as a function of the number of elements biased. The one- and two-element cases were fed in the far field, while the other data points are for focal-point feeds.

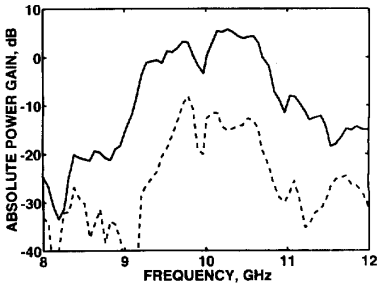

Fig. 9. Measured absolute power gain as a function of frequency for the 24-element planar lens amplifier in the biased-on (solid line) and biased-off (dashed line) conditions. The isolation is greater than 17dB over a 320 MHz bandwidth and is 21 dB at 10.25 GHz.

designed. The lens diameter is around $4\lambda_0$, the focal length is 25 cm, and $F/D = 2$. A triangular inter-element spacing increases the element density. The output side has uniform inter-element spacing of $0.75\lambda_0$ in the horizontal direction and $0.90\lambda_0$ in the vertical direction. The relatively large spacing in the vertical direction is required to accommodate the via holes connecting the feed-side and output-side ground planes crucial to the isolation and stability of the lens amplifier. The microstrip patch antennas are fed on the non-radiating edge with 100–Ω input impedance at resonance. The output element polar coordinates with respect to the lens axis are (r, ϕ_e), and the input element coordinates are (ρ, ϕ_e), where the radial distance ρ is given by a modified form of (1) as

$$\rho = r\left[\frac{F^2 - r^2 \sin^2\theta_0 \cos^2\phi_e}{F^2 - r^2}\right]^{1/2}. \tag{7}$$

The line length connecting input elements to output elements is similarly modified from (2)

$$W = F + W_0 - 1/2[F^2 + \rho^2 - 2\rho F \sin\theta_0 \cos\phi_e]^{1/2} - 1/2[F^2 + \rho^2 + 2\rho F \sin\theta_0 \cos\phi_e]^{1/2}. \tag{8}$$

The design of the single-stage PHEMT amplifier was performed using Hewlett Packard's Microwave Design System to account for all discontinuities in the amplifier layout. A microstrip amplifier without antennas as loads was tested on an HP 8510B network analyzer. The peak gain is 13.1 dB at 9.92 GHz, and its 3-dB bandwidth is 1.4 GHz. The peak gain of the amplifier used in the two-dimensional lens is 3.3 dB higher than the amplifier used in the linear 7-element lens. With a single element of the lens biased, a free-space gain measurement yielded an amplifier gain of 12.9 dB, indicating good agreement with the network analyzer measurements.

We biased several symmetrical configurations of lens elements to study how the lens insertion gain (or loss) is affected by the number of elements. The results, plotted in Fig. 8, show a dramatic improvement in absolute power gain as the number of elements increases. The one- and two-element results were obtained by biasing the center two elements of the lens amplifier and feeding them from the far field. These two elements have identical delay line lengths. The free-space measurement established the fact that the PHEMT amplifiers contribute 12.9 dB of gain, but the lens suffers over 15 dB of insertion loss because the feed is located in the far field, and most of the input power is not captured by the lens. A dramatic decrease in the lens insertion loss occurs when the lens is fed at its focal point for the cases when four or more elements are biased, showing that feed efficiency of free-space amplifiers is improved when fed as a lens. With all 24 elements biased, the lens delivers 5.7 dB of absolute power gain. The lens frequency response is tested using a Hewlett Packard HP 71500/80200 microwave transition analyzer with a standard-gain horn illuminating the lens at its focal point and another horn receiving the power in the far field of the lens. The resulting frequency plot in Fig. 9 shows a bandwidth of 320 MHz over which the isolation is at least 17 dB. A peak isolation value of 21 dB occurs at 10.25 GHz. The frequency response of the 24-element lens is broader than that of the 7-element lens and has two peaks. One peak is at 10.25 GHz and the other peak, 2.1 dB lower than the first, is at 9.7 GHz. We believe the reason for this is the inadvertent variation in the resonant frequency of the patches. Namely, for some input-side elements, the radiating edges are closer to their neighboring ground planes, altering the effective dielectric constant of these patches.

An estimate of the feed efficiency of the lens was performed by measuring the peak power reflected by the input side of the biased-on lens, and comparing that power to the peak power reflected off of a metal plate of the same dimensions as the lens. For both measurements, the horn feed was placed on the focal arc at an angle of 30° to avoid blockage by the horn. The peak reflected power was measured at $-30°$ as expected, and 4 dB more power was reflected by the metal plate than by the lens. Therefore, we estimate that about 39% of the power incident on the lens is reflected and not coupled into the amplifiers. Increasing the element density, matching the resonant frequency of all elements, and reducing the reflection due to the isolating ground planes should reduce the reflected power.

IV. Grid Oscillator Feed Design

A planar grid oscillator was designed to feed the two-dimensional lens amplifier array. The theory presented in [10] was used, which is based on a full-wave analysis of a single unit cell of the structure. For a given geometry, the metallization is divided into a number of rooftop basis

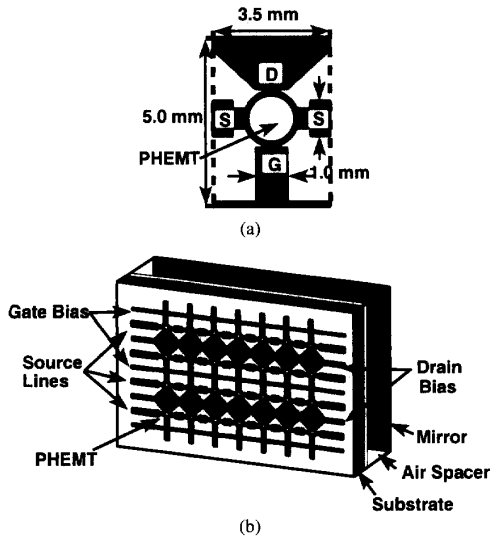

Fig. 10. A grid oscillator unit cell is shown in (a), where the solid lines are electric walls and the dashed lines are magnetic walls. The 28–element grid oscillator is shown in (b).

functions and a voltage generator is inserted across the gap in place of a 1-port active device. The moment method is then used to determine the current on the entire structure, and the ratio of the voltage across the gap to the current through the gap is the driving-point impedance seen by the active device. This analysis is extended to a two-port device, such as a transistor, yielding a two-port characterization for the passive part of the grid (the metal geometry, the dielectric, and radiation into free space). An appropriate model for the active device is then connected to this linear network to analyze the behavior of the grid oscillator.

In order to match the narrow-band frequency response of the two-dimensional lens amplifier, a grid oscillator operating at 10 GHz is required. In the design, small-signal s-parameters were used to model the Avantek ATF-35576 PHEMT's, the devices selected for fabricating the oscillator. Simulations indicate that a structure with one dipole and one bow-tie radiating element on a 2.54-mm thick Duroid substrate with a relative permittivity of 10.5 results in an oscillation frequency near 10 GHz. The unit cell of the structure is shown in Fig. 10(a), and the entire grid oscillator is shown in Fig. 10(b). According to the simulations, a mirror placed 3 mm behind the dielectric results in an oscillation frequency of 10 GHz. The fabricated grid requires a grid-to-mirror spacing of 5 mm to tune the frequency to 10.0 GHz. We observe a gate-bias tuning bandwidth of 225 MHz with less than 3 dB change in output power. The grid oscillator can be electrically tuned over the operating bandwidth of the lens amplifier array. The 28-element grid oscillator has an effective radiated power of 22 dBm measured in the far field.

V. Two-Level Power Combiner Performance

For broadside radiation, we mount the grid oscillator along the optical axis of the two-dimensional lens amplifier array in an anechoic chamber. The best output power is produced

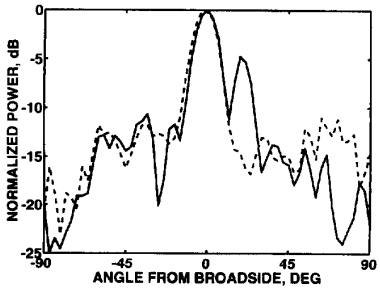

Fig. 11. Measured antenna patterns for the 24–elemment lens amplifier array fed by the grid oscillator at the focal point. E-plane (solid line) and H-plane (dashed line) beamwidths are both around 11°.

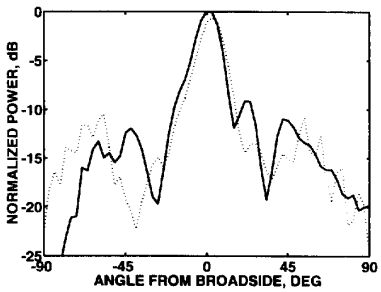

Fig. 12. Measured E-plane pattern for the 24–element lens amplifier array fed by a horn at the focal point at 10.25 GHz (solid line) and 9.70 GHZ (dotted line).

when the grid oscillator is 15 cm away from the lens. Since the effective size of the grid oscillator is approximately 2.0 cm by 2.5 cm, we expect the optimum feed distance to be closer than the design focal length. The bias of the grid oscillator is $V_{ds} = 2.0$ V, $I_{ds} = 210$ mA, and $V_{gs} = -1.05$ V, and generates 150 mW effective radiated power (ERP) at 10.25 GHz. The lens transistors are biased in parallel at $V_{ds} = 2.5$ V, $I_{ds} = 400$ mA, and $V_{gs} = -0.25$ V. When the oscillator feeds the lens at its optimum feed point, the lens ERP is 525 mW, showing an insertion gain of 5.4 dB. The isolation of the lens is tested by increasing the gate bias to -2.0 V, resulting in 2 mA total drain current. The isolation ratio at 10.25 GHz is 21 dB. A cross-polarization ratio of 23 dB for the lens is found by polarization mismatching the grid oscillator feed and the receive horn with respect to the input and output of the lens, respectively. E-plane and H-plane patterns of the lens fed at broadside are shown in Fig. 11. The main lobe 3-dB beamwidths of the E- and H-plane patterns are approximately 11°, which is in good agreement with a theoretical value of 11.3° for a uniformly driven array. The H-plane pattern side lobe level is better than -12 dB, but the E-plane pattern exhibits a significant lobe at $+20°$. We believe the cause of this lobe is an asymmetry in the near field radiation pattern of the grid oscillator. We replaced the grid oscillator feed with a horn and measured the E-plane radiation patterns of the lens at 10.25 GHz and 9.7 GHz. The resulting patterns, shown in Fig. 12, indicate that the lobe at $+20°$ is reduced by 5 dB at 10.25 GHz, and essentially disappears at 9.7 GHz.

Beamsteering is performed by positioning the grid oscillator at various angles off of broadside along the focal arc. Fig. 13

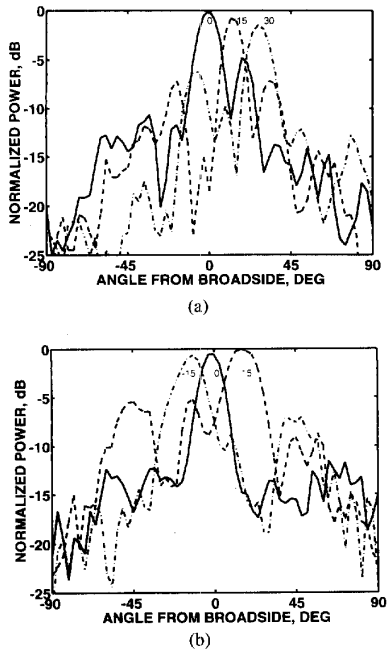

Fig. 13. Measured beamsteering patterns for the 24–element lens amplifier. (a) The E-plane main lobe power variation is 2 dB over a 30° scan range, and (b) the H-plane main lobe power variation is 1 dB over a ±15° scan angle.

shows the measured beamsteering in both planes. The beam can be steered in the E-plane by 30° with less than 2 dB power variation. The asymmetric side lobe in the broadside-fed E-plane pattern is reduced when the lens is fed from the +15° and +30° feed points, as expected. Grating lobes are observed for scan angles greater than 24° in the H-plane beamsteering measurement due to the large inter-element spacing.

VI. Conclusion

A two-dimensional, 24-element planar lens amplifier and a grid oscillator are integrated into a two-level quasi-optical power combining system. The amplifier demonstrates an isolation (on/off ratio) of 21 dB and a cross-polarization ratio of 23 dB at a center frequency of 10.25 GHz. When fed by a 28-element grid oscillator, an effective radiated power of 525 mW is measured. The grid oscillator is designed using a full-wave theory and is tunable over the pass band of the amplifier. The lens has an insertion power gain of 5.7 dB. The output beam of the two-level free-space combiner can be steered in both E- and H-planes. E-plane beamsteering to a 30° scan angle is demonstrated with less than 2 dB of main lobe power variation. H-plane beamsteering of up to 24° is measured. Another lens amplifier, a 7-element linear array fed by a horn, has a center frequency of 9.7 GHz and an isolation figure of 29 dB. Scanning angles up to 30° produce less than 1 dB of main lobe power variation when the linear lens array is fed along its focal arc. These lens systems are useful for amplification, focusing and beamsteering applications with solid state power generation.

Acknowledgment

J. Schoenberg holds an Air Force Institute of Technology Civilian Institution Program fellowship. The authors also thank Hewlett Packard for their generous equipment donations and the Rogers Corporation for substrate donations.

References

[1] Z. B. Popović, R. M. Weikle, M. Kim, and D. B. Rutledge, "A 100-MESFET planar grid oscillator," *IEEE Trans. Microwave Theory Tech.*, vol. 39, pp. 193–200, Feb. 1991.
[2] J. Birkeland and T. Itoh, "A FET oscillator element for spatially injection locked arrays," *IEEE 1992 MTT-S Symp. Dig.*, vol. 3, June 1992, pp. 1535–1538.
[3] M. Kim, *et al.*, "A grid amplifier," *IEEE Microwave Guided Wave Lett.*, vol. 1, pp. 322–324, Nov. 1991.
[4] T. Mader, J. Schoenberg, L. Harmon, and Z. B. Popović, "Planar MESFET transmission wave amplifier," *IEE Electron. Lett.*, vol. 29, no. 19, pp. 1699–1701, Sept. 16, 1993.
[5] D. T. McGrath, "Planar three-dimensional constrained lenses," *IEEE Trans. Antennas Propagat.*, vol. 34, pp. 46–50, Jan. 1986.
[6] ——, "Slot-coupled microstrip constrained lens," *Proc. Antenna Appl. Symp.*, Sept. 1987.
[7] J. S. H. Schoenberg and Z. B. Popović, "Planar lens amplifier," *IEEE MTT-S Symp. Dig.*, vol. 1, 1994, pp. 429–432.
[8] A. Banalli, C. Thng, and K. C. Gupta, "CAD of microstrip patch antennas," *MICROPATCH, Microstrip Designs, Inc.*, 1993.
[9] R. T. Webster, A. J. Slobodnik, and G. A. Roberts, "Monolithic InP HEMT *V*-band low noise amplifier," *IEEE Microwave Guided Wave Lett.*, vol. 2, pp. 236–238, June 1992.
[10] S. C. Bundy and Z. B. Popović, "Analysis of planar grid oscillators," *IEEE 1994 MTT-S Symp. Dig.*, vol. 2, pp. 827–830.

Jon S. H. Schoenberg (M'86) was born in Schenectady, NY in 1963. He received the B.S. degree in electrical engineering from Cornell University, Ithaca, NY and the M.S.E.E. degree from Northeastern University, Boston, MA, in 1985 and 1989, respectively. He is pursuing the Ph.D. degree in electrical engineering at the University of Colorado, Boulder.

From 1985 to 1989, he was assigned to the Electromagnetics Directorate of the Rome Air Development Center, where he performed FET modeling for MMIC's. In addition, he performed high speed photonic switching research and initiated a development effort for V-band low noise and power amplifiers on InP substrates. In 1989, he joined the faculty of the Air Force Academy's Electrical Engineering Department. His research interest include quasi-optical amplifiers, high speed devices, and array beamforming and beamsteering.

Captain Schoenberg is a member of the IEEE MTT and Electron Devices societies, and Eta Kappa Nu.

Scott C. Bundy (S'92) was born November 15, 1966, in Denver, CO. He received the B.S. and M.S. degrees in electrical engineering at the University of Colorado, Boulder, in 1990 and 1992 respectively. He is pursuing the Ph.D. degree in electrical engineering at the same university.

He has held summer positions at the 3M Company and at Los Alamos National Laboratory. His research interests include quasi-optical oscillators and moment method analysis of periodic grid structures.

Zoya Basta Popović, for a photograph and biography, see page 1826 of the September issue of this TRANSACTIONS.